Available online at www.sciencedirect.com
SCIENCE DIRECT
ELSEVIER
Journal of the European Ceramic Society 26 (2006) 2889–2898
ECERS
www.elsevier.com/locate/jeurceramsoc

# Grain size and grain boundary-related effects on the properties of nanocrystalline barium titanate ceramics

V. Buscaglia [a], M.T. Buscaglia [a], M. Viviani [a], L. Mitoseriu [b,c,*], P. Nanni [a,b], V. Trefiletti [d], P. Piaggio [e], I. Gregora [f], T. Ostapchuk [f], J. Pokorný [f], J. Petzelt [f]

[a] *Institute for Energetics and Interphases, National Research Council, Via de Marini 6, Genoa I-16149, Italy*
[b] *Department Chemical and Process Engineering, University of Genoa, P-le Kennedy 1, Genoa I-16129, Italy*
[c] *Department of Solid State and Theoretical Physics, Al. I. Cuza University, Bv. Carol I 11, Iasi 700506, Romania*
[d] *Institute of Macromolecular Materials, Department of Genoa, National Research Council, Via De Marini 6, Genoa I-16149, Italy*
[e] *Department of Chemistry and Industrial Chemistry, University of Genoa, Via Dodecaneso 31, Genoa I-16146, Italy*
[f] *Institute of Physics, Academy of Sciences, Na Slovance 2, 18221 Praha 8, Czech Republic*

Available online 20 March 2006

**Abstract**

Dense nanocrystalline $BaTiO_3$ ceramics with grain size (GS) down to 50 nm were studied by X-ray diffraction (XRD), differential scanning calorimetry (DSC), impedance spectroscopy and Raman spectroscopy. A continuous reduction of the tetragonal distortion towards the pseudo-cubic state was obtained when the GS was reduced. Therefore, even the finest structure (ceramic with average GS of 50 nm) is still non-centrosymmetric. The dielectric constant ($K$) shows relative thermal stability in a large range of temperatures and is strongly depressed in the nanocrystalline ceramics, in comparison with the micrometric ones ($K$ being below 1000 for the ceramic with 50 nm GS). The losses are smaller than 5% in the frequency range of $10^2$–$10^6$ Hz and temperatures below 200 °C. As the GS decreases, the structural phase transitions assume a more diffuse character. A decrease of the Curie temperature with reducing the GS was confirmed by X-ray, calorimetric and permittivity data. The Raman spectra collected for the range 80–800 K provided evidence for the presence of all the crystalline phases of $BaTiO_3$, as in single-crystal and micrometric ceramics; a few differences can be attributed to GS effects and to the high density of the non-ferroelectric grain boundaries. Evidence for the different phase transitions were provided by the disappearance of some bands and by anomalies in positions and intensities of selected Raman modes. The overall properties of the nanocrystalline $BaTiO_3$ ceramics can be explained as a combination of intrinsic effects, associated with the decrease of tetragonality and heat of transition with reducing GS, and extrinsic contributions due to the non-ferroelectric grain boundaries causing a "dilution" of the ferroelectric properties.


*Keywords:* Grain size; Grain boundaries; Spectroscopy; Dielectric properties; $BaTiO_3$

## 1. Introduction

Barium titanate $BaTiO_3$ (BT) is one of the ferroelectrics used at the largest scale as base material for multilayer ceramic capacitors, piezoelectric transducers, wireless communication devices, pyroelectric elements and positive temperature coefficient (PTC) sensors. The tendency of the electronic industry towards miniaturization and the need to achieve higher performances in smaller structures lead to high interest in understanding the changes of properties while passing from bulk to the nanosized systems, as well to determine the ultimate structure (particle or grain size (GS), thickness, etc.) whilst still preserving ferroelectric properties.[1,2] The dielectric properties of BT ceramics as a function of GS were extensively investigated, starting in the 1960s, and explained in terms of GS-dependence of the residual stresses, domain wall density, depolarizing fields and surface/interface effects.[1,3–7] In spite of the large volume of literature dedicated to GS effects in BT ceramics, reliable data have been mostly obtained for ceramics with GS $\geq$300 nm, due to the difficulty of producing fully dense ceramics below this size. Results previously reported for samples with smaller grains are likely to be strongly affected by the high degree of porosity.[1]

Dense BT ceramics with grains below 100 nm have been obtained only in recent years, using special densification methods like ultra-high pressure sintering in a multianvil press (GS

* Corresponding author. Tel.: +40 32 144760; fax: +40 32 213330.
*E-mail address:* lmtsr@uaic.ro (L. Mitoseriu).

0955-2219/$ – see front matter © 2006 Elsevier Ltd. All rights reserved.
doi:10.1016/j.jeurceramsoc.2006.02.005

down to 70 nm, 98% relative density)[8] or by a combined sintering method (GS down to 90 nm, 99% relative density).[9] A further step towards the production of dense nanocrystalline BT ceramics was made quite recently by using the spark plasma sintering (SPS) technique. Ceramics with GS down to 50 nm and 97% relative density[10,11] were produced by this process. Dielectric measurements[8–10] have shown a significant lowering of the relative dielectric constant in these ceramics in comparison to the coarse ones. This behaviour was interpreted in terms of the presence of a low-permittivity non-ferroelectric GB layer. Since in the studies mentioned above no secondary phases were found, it follows that such a "dead" layer could correspond either to a paraelectric state of BT or to a polar non-switchable state (frozen dipoles) at the surface of the grains.[8–11] However, the real nature of this "modified" region at the GBs and its effect on the properties of the nanosystems is still unclear.

At high temperature BT has a paraelectric cubic (C) perovskite phase; as the temperature decreases, it undergoes three successive transitions to ferroelectric phases with tetragonal (T), orthorhombic (O) and rhombohedral (R) symmetries at around 403, 278 and 183 K, respectively (values characteristics for the single-crystal).[12–14] All these structural modifications correspond to small deformations of the cubic lattice. With decreasing GS, the phase transitions assume a more diffuse character and display a lower transition enthalpy (in particular the R–O and the O–T transitions).[1,4] Although there is not general agreement, there are indications that the relative stability of the different phases is also affected by GS: the C–T transition is shifted towards lower temperatures and the O–T transition to higher temperatures with decreasing GS.[1,9] The possible coexistence of different BT structural modifications in submicron ceramics at room temperature (T and O, C and T) has been also proposed to explain some anomalies observed in the X-ray diffraction (XRD) patterns or discrepancies between XRD and Raman data.[4,15–17] In coarse BT ceramics, the location of the phase transitions is indicated by anomalies of the relative dielectric constant and of other physical properties.[16] However, in nanocrystalline ceramics, this method is less sensitive because the anomalies corresponding to the R–O and R–T transitions are very weak or even absent.[1,12–14] Raman spectroscopy gives information on the composition and structure of materials, being able to detect modifications of short-range order related to changes in the chemical bond length and angles, thus representing a very useful tool to study order–disorder phenomena and phase transitions.[18] Due to its ability to detect local dynamic symmetry in small regions (coherence length lower than 2 nm[19]), it is particularly useful for probing phase transitions which are barely detectable by other methods, as in case of relaxors,[18,20] to prove non-centrosymmetric local structures in apparent pseudo-cubic nanopowders[21] and nanopolar regions in incipient ferroelectrics[22] or composition-induced structural transitions between rhombohedral, monoclinic and tetragonal phases in $Pb(Zr,Ti)O_3$ in the range of the famous and still controversial morphotropic phase boundary composition.[23] In addition, in case of ultrafine BT structures, mostly the ferro–para phase transition was investigated and no information on the other low-temperature transitions was found in literature.[1] In the present work, Raman spectroscopy was used in addition to the XRD, calorimetric and dielectric investigations in order to find evidence of the structural phase transitions in dense nanocrystalline $BaTiO_3$ ceramics.

## 2. Experiment

Ultrafine $BaTiO_3$ powders were prepared by precipitation from an aqueous solution of the metallic chlorides in strong alkaline conditions (pH 14) as described elsewhere.[24,25] The specific surface area of the powders was ≈30 $m^2$/g, corresponding to primary particles of ≈35 nm. The Ba/Ti ratio of the powders was controlled to $1.00 \pm 0.01$, as confirmed by inductively coupled plasma spectroscopy. The main impurities in the powders were Na (≈400 ppm) and Sr (below 50 ppm). The powders were then sintered as disks of 1.2 cm diameter and 0.1–0.2 cm thickness by SPS (Dr. Sinter 2050, Sumitomo Coal Mining Co., Tokyo, Japan).[26] The powder was poured into a graphite die, heated at 200 °C/min up to the sintering temperature with an applied pressure of 100 MPa and held at constant temperature (800–1000 °C) for 2–5 min. Rapid heating is provided by a pulsed DC current. The electric power was switched off and the sample cooled at about 400 °C/min with no pressure. The as-sintered ceramics were finally polished and then annealed in air for 1–10 h at a temperature of 700 or 800 °C, depending on GS. This treatment should guarantee the relief of residual stresses (arising either from the SPS process or from polishing), the removal of surface carbon contamination and the elimination of excess oxygen vacancies possibly produced during SPS. Three nanocrystalline ceramics with different GS were prepared by SPS: ∼50, ∼100 and ∼300 nm. Coarser ceramics were obtained by conventional pressureless sintering in air from the same powders: ∼500 nm, sintered at 1285 °C and ∼1200 nm, sintered at 1310 °C. Like the SPS samples, the coarse ceramics were annealed after polishing to minimize residual stresses arising from polishing.

The density of the ceramics was measured by the Archimedes method and a theoretical density of 6.02 g/$cm^3$ was assumed. The relative density was ≥97% for all samples, with the exception of the sample with GS ≈ 500 nm (94%). Microstructures of the samples were examined by scanning electron microscopy (SEM) both on fracture surfaces and on polished surfaces after chemical or thermal etching. The average GS was determined as the mean intercept length on the basis of ∼250 intercepts. XRD was used to check the phase purity and to determine the lattice parameters by means of Rietveld refinement. The patterns, including all reflections from (1 0 0) to (4 0 0), were collected from polished surfaces at room temperature with Co Kα radiation, using a $2\theta$ step of 0.03° and a sampling time of 10 s. XRD patterns from a narrower angular range containing the (1 0 1), (1 1 1) and (2 0 0) reflections were also collected for a sample with GS = 50 nm from room temperature to 473 K using a diffractometer equipped with a heating chamber. Differential scanning calorimetry (DSC) measurements were performed on samples of ∼100 mg cut from the sintered disks in the range 253–453 K at a heating/cooling rate of 10 K/min. The enthalpy of transition was estimated from the area of the DSC peaks. For the electrical measurements, Pd–Ag electrodes were

applied on the upper and lower surfaces of the sintered disks after polishing. The permittivity measurements were carried out in air at $10^2$–$10^6$ Hz using an impedance analyzer (Solartron 1260) in the temperature range 40–180 °C (heating/cooling rate of 0.5 °C/min). FT-Raman spectra obtained from crushed nanocrystalline ceramics placed in a capillary were collected from room temperature up to 525 K using a Bruker RFS100 spectrometer equipped with Nd-YAG laser (1064 nm). The unpolarized Raman spectra in back scattering geometry were obtained from the surface of nanocrystalline ceramics using a micro-Raman spectrometer (RENISHAW RM 1000) with a laser beam of 514.5 nm focused to a spot of 1–2 μm in diameter, with a depth of field of about 10 μm. The spectra were recorded in the spectral range of 80–1000 $cm^{-1}$ at temperatures between 80 and 800 K, using LINKAM thermal cells. Due to the instrumental cut-off, soft modes with wave numbers below 80 $cm^{-1}$ could not be observed.

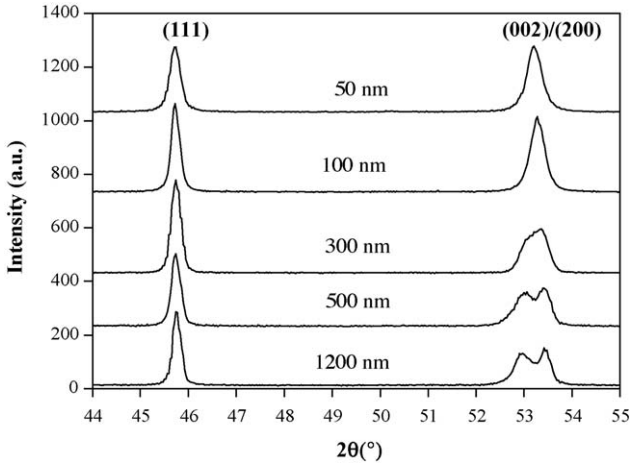


Fig. 2. Part of the X-ray diffraction pattern (Co Kα radiation) for $BaTiO_3$ ceramics with different grain size (50–1200 nm) at room temperature.

## 3. Results and discussions

### 3.1. Microstructure and crystalline symmetry

The average GS of the series of samples determined by SEM was 51, 94, 282, 530 and 1200 nm. Representative SEM pictures illustrating microstructures of samples with various GS are shown in Fig. 1. The crystallite size of the nanocrystalline samples was also estimated from the broadening of the (1 1 1) and (2 2 2) XRD peaks, after correction for instrumental broadening, by means of the Scherrer formula. The obtained values are 54 and 96 nm, respectively, in a good agreement with the SEM observations. Measurement of the crystallite size before and after the post-annealing process did not reveal any significant change, meaning that no appreciable grain growth occurred during this process. Secondary phases, if any, are below the XRD detection limit (≈1%).

The portion of the diffraction pattern corresponding to the (1 1 1) and to the (2 0 0)/(0 0 2) reflections is reported in Fig. 2

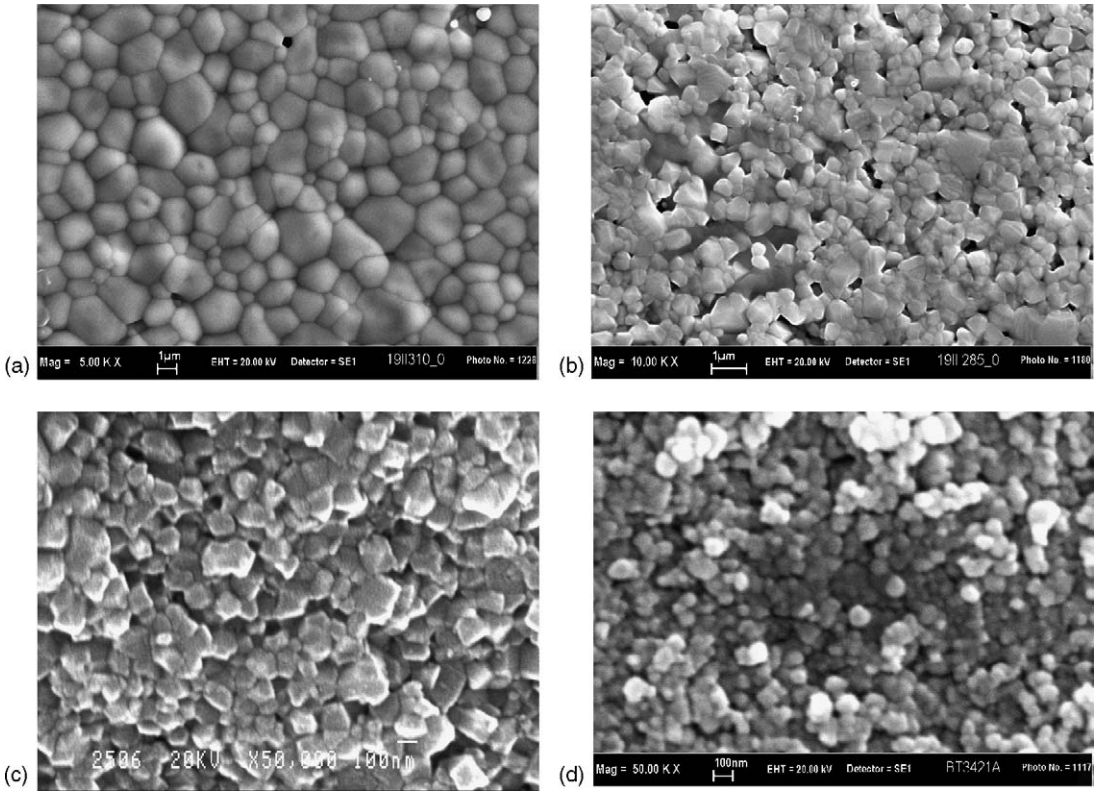


Fig. 1. SEM micrographs for $BaTiO_3$ samples having the grain sizes: (a) GS = 1200 (thermal etching); (b) GS = 500 (thermal etching); (c) GS = 100 (fractography); and (d) GS = 50 (chemical etching).

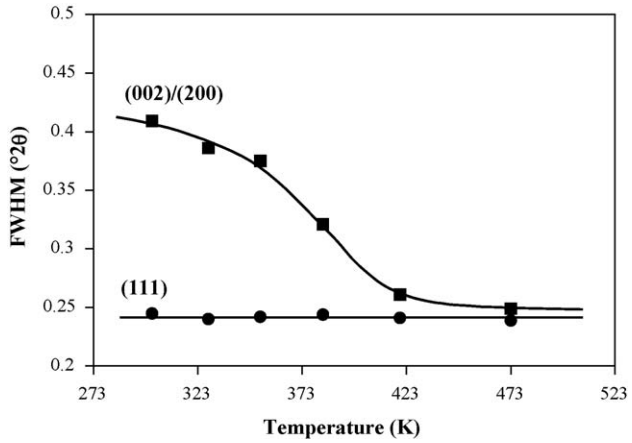


Fig. 3. Apparent full-width at half maximum (FWHM) of the (1 1 1) and (2 0 0)/(0 0 2) reflections obtained for a $BaTiO_3$ ceramic with grain size of 50 nm as a function of temperature.

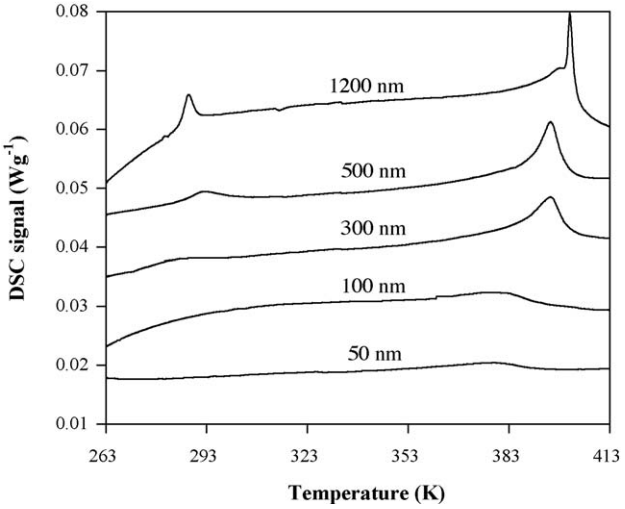


Fig. 4. Differential scanning calorimetry traces for $BaTiO_3$ ceramics illustrating the dependence of orthorhombic–tetragonal (O–T) and tetragonal–cubic (T–C) structural transitions on the grain size.

as a function of GS. The splitting of the (2 0 0)/(0 0 2) lines gradually decreases, meaning that the tetragonality *c*/*a* (*a* and *c* being the lattice parameters) is progressively reduced with decreasing GS.[10] A good fit of the whole diffraction pattern of samples with GS ≥300 nm could be obtained by the Rietveld method using the tetragonal structure. The splitting is no longer observed for the nanocrystalline ceramics with GS ≈ 100 nm and GS ≈ 50 nm and the patterns apparently correspond to (Pm3m) cubic symmetry. However, an indication of the existence of low crystalline symmetry is provided by the pronounced broadening of most of the diffraction peaks in comparison to the (h h h) reflections, which are not subjected to splitting during the C–T transformation. Such anomalous broadening disappears at higher temperature when the cubic structure is expected to be stable. The evolution of the apparent full-width at half maximum (FWHM) of the (1 1 1) and (2 0 0)/(0 0 2) XRD lines with temperature is shown in Fig. 3 for the ceramic with GS ≈ 50 nm. A progressive decrease of the FWHM with increasing temperature and the rather diffuse character of the phase transition can be observed. The apparent pseudo-cubic structure becomes fully cubic above 423 K, when the FWHM of the (1 1 1) and (2 0 0) lines are comparable (the (0 0 h) reflections are not permitted in the (Pm3m) symmetry). From the data of Fig. 3, the average Curie temperature can be estimated to be ≈378 K. Thus, the apparent cubic XRD pattern exhibited by the nanocrystalline samples at room temperature is the consequence of a very small distortion from the cubic lattice and of the broadening effect related to the small GS. However, the true symmetry of the polar phase in the nanocrystalline samples (GS ≈ 50 nm and GS ≈ 100 nm) at room temperature cannot be determined unambiguously from the present XRD results alone: Rietveld refinement gave a comparable fit with either T or O symmetry at room temperature. In any case the distortion of the perovskite structure from the ideal cubic lattice (defined as the ratio of the O–O distance along the *z*-axis to the O–O distance along *x*- and *y*-axes in the $TiO_6$ octahedron) is very low for the sample GS ≈ 50 nm: *c*/*a* ≈ 1.003 in comparison to the spontaneous strain observed in coarse ceramics: *c*/*a* = 1.01.[4,12–14]

### 3.2. Differential scanning calorimetry data

Typical DSC traces for the different ceramics are reported in Fig. 4. For the coarser sample, the endothermic features near 283 and 403 K can be attributed to the O–T and T–C transitions, respectively. It is evident that, with decreasing GS, the DSC peaks are progressively weakened and broadened. As a result, the corresponding heat of transition is reduced. For the sample with GS ≈ 300 nm, the enthalpies of the O–T and T–C transformations are 23 and 161 J/mol, respectively. For the sake of comparison, the reference values reported for single-crystals are 92 and 210 J/mol, respectively.[12–14] For the finest ceramic (GS ≈ 50 nm), the enthalpy of the T–C transition is reduced to only 20% of the single-crystal value, being ≈45 J/mol. The average T–C transition temperature corresponding to the maximum of the DSC peak is progressively shifted towards lower values, from 400 K for GS ≈ 1200 nm to 378 K for GS ≈ 50 nm (Fig. 4). The O–T transition is no longer observed in the case of nanocrystalline ceramics (GS ≤ 100 nm). Although the most likely reason for the apparent absence of the phase transition is the instrumental detection limit (5–10 J/mol), the possible suppression of one of the polar phases in the nanocrystalline ceramics cannot a priori be discarded.

The evolution of the shape of the XRD peaks (Figs. 2 and 3) and the shift of the T–C transition temperature determined by DSC (Fig. 4) cannot be explained on the basis of a simple model of the ceramic corresponding to ferroelectric grain cores with the same properties of a macroscopic single-crystal separated by a GB layer with cubic structure (*c*/*a* = 1), even assuming that the fraction of the ferroelectric phase decreases with decreasing GS. On the contrary, the above results indicate a gradual reduction of the spontaneous tetragonal distortion (directly related to the spontaneous polarization) and of the non-centrosymmetric character of the BT lattice with decreasing GS, and support the existence of an intrinsic size effect in BT ceramics.[10]

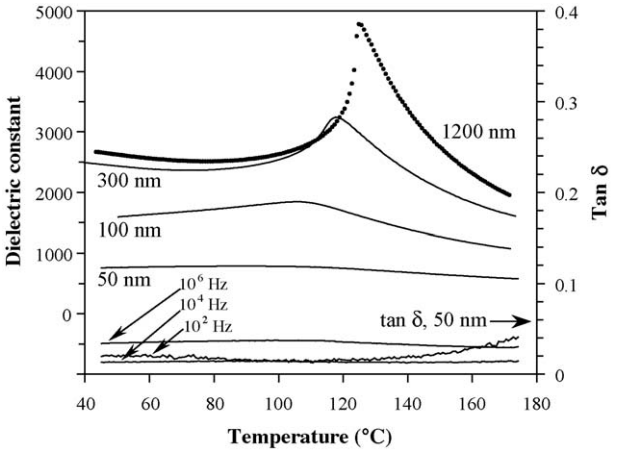


Fig. 5. Relative dielectric constant ($K$) at 10 kHz and loss tangent ($\tan\delta$) of $BaTiO_3$ ceramics with various grain sizes (GS = 50, 100, 300, 1200 nm) as a function of temperature. Tan $\delta$ is reported for the 50 nm sample at three frequency values: $10^2$, $10^4$ and $10^6$ Hz.

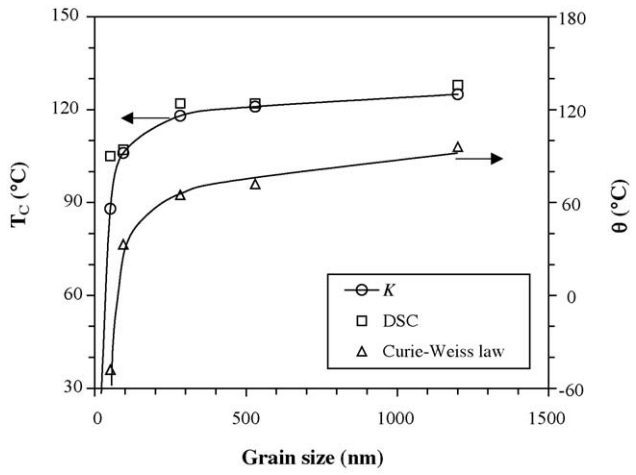


Fig. 6. Critical temperatures of $BaTiO_3$ ceramics as a function of grain size. Curie temperature ($T_C$) was determined from (◯) dielectric measurements; (□) DSC measurements; and (△) Curie–Weiss temperature ($\theta$).

### 3.3. Dielectric characteristics

The relative dielectric constant ($K$) and the dielectric losses ($\tan\delta$) of the $BaTiO_3$ ceramics with GSs of ≈50, 100, 300 and 1200 nm are reported in Fig. 5. A dielectric anomaly is clearly observable for all samples, indicating ferroelectric behaviour. The permittivity is strongly depressed for fine-grained samples. For example, at the temperature of 70 °C and frequency $f = 10$ kHz, $K = 2520$ for GS ≈ 1200 nm, $K = 2200$ for GS ≈ 300 nm, $K = 1680$ for GS ≈ 100 nm, and $K = 780$ for GS ≈ 50 nm. These values are lower than those reported by Frey et al.[15] but comparable with the trend found by Arlt et al.[4] The dielectric permittivity of the nanocrystalline samples is remarkably less sensitive to temperature in contrast to the coarse ceramics. The dielectric losses of the fine-grained ceramics (50–300 nm) are rather small, <5% in the whole frequency range and comprised between 1 and 2% in the range (3–300) kHz. These figures give an indication of the dielectric quality of the samples. The losses ($\tan\delta$) of the finest sample GS ≈ 50 nm, selected as representative, are reported in Fig. 5. Despite the significant broadening of the permittivity peak, the position of the maximum of the permittivity can be still considered as an indication of the ferroelectric–paraelectric transition temperature, $T_C$. The Curie temperature is progressively lowered with decreasing GS, from 125 °C (GS ≈ 1200 nm) to ∼90 °C (GS ≈ 50 nm), as shown in Fig. 6. For a given GS, $T_C$ is almost unaffected by frequency, the variations being within 1–2 °C. In the paraelectric region, the permittivity of all fine-grained ceramics closely follows the Curie–Weiss (CW) law for $T > 125$ °C. The CW temperature ($\theta$) gradually decreases with decreasing GS: from 96 °C (GS ≈ 1200 nm) to −48 °C (GS ≈ 50 nm), as shown in Fig. 6. The Curie constant ($C$) is nearly the same, $(1.5–1.6) \times 10^5$ K, for all samples with GS ≥ 100 nm. For the GS ≈ 50 nm sample, $C$ is slightly lower: $1.3 \times 10^5$ K. The CW temperature and the Curie constant are practically independent of frequency in the range 3 kHz–1 MHz. At lower frequencies a moderate increase of $C$ (up to $1.7 \times 10^5$) and a decrease of $\theta$ (down to −76 °C for GS ≈ 50 nm) is observed. The diffuse character of the ferroelectric–paraelectric phase transition with a broad maximum at ∼90 °C found in the finest ceramics GS ≈ 50 nm is related to the local inhomogeneity of the system. Due to the local tetragonality changes related to the GS distribution, various distributed Curie temperatures are expected locally and as a result there are very broad features in the dielectric and calorimetric characteristics of the nanocrystalline ceramics (Figs. 4 and 5). As mentioned before, the gradual reduction of the tetragonal distortion and of the heat of transition with decreasing GS support the existence of an intrinsic size effect in BT ceramics.[10] However, a high density of non-ferroelectric GBs ("dead layer") can be responsible for extrinsic size effects. For instance, the depression of the permittivity in nanocrystalline BT ceramics and the strong reduction of the CW temperature can be largely ascribed to a "dilution" effect of the non-ferroelectric GBs.[8,10] Using an effective permittivity model, the thickness of the "dead layer" in the present ceramics was estimated to be of 2–3 nm.[10] Thus, the volume fraction of the grain-boundary dead layer increases with decreasing GS and attains a value of 10–20% for a GS of 50 nm. The non-ferroelectric GBs are probably responsible also for some peculiar features found in the Raman activity.[27]

### 3.4. Raman spectroscopy

In spite of the large number of studies, the allocation of the vibration modes in BT is still a matter of debate.[28–32] In the cubic phase, the BT lattice dynamics is strongly anharmonic and the soft mode is overdamped.[28–35] At the C–T phase transition, the triply degenerate soft mode splits into well-separated components A1(TO1) and E(TO1) at ∼260 and ∼50 $cm^{-1}$, respectively.[32] In the T phase, the overdamped E-component of the soft mode (responsible for the high dielectric anisotropy at room temperature) continues its softening down to the T–O transition, when the double-degenerate E-component splits into B1 (∼250 $cm^{-1}$) and overdamped B2 (∼60 $cm^{-1}$) components.[32,33] At the O–R transitions these components

change into underdamped doubly degenerate E-component of the stiffened component at $\sim$250 cm$^{-1}$.[33] The stiffened A1 component keeps its wavenumber at $\sim$260 cm$^{-1}$ across all the phase transitions. It is worth noting that these values for the eigenfrequencies are approximate, due to the lack of data for monodomain single-crystals in the low symmetry phases (R and O) and to the ambiguous interpretation of the unpolarized spectra of polydomain structures. This scenario of the soft mode behaviour correlates with the temperature dependence of the static permittivity[12–14] and corresponds to the symmetry changes of BT.[34] Some specific effects, not present or of marginal importance in single-crystals, have to be considered for the interpretation of Raman spectra in polycrystalline systems (as ceramics and films). Due to the random grain orientations, the directions of the phonon wave vectors are randomly distributed from one grain to another with respect to the crystallographic axes, causing relatively broader Raman modes as a result of mixing and long-range electrostatic force effects.[31] By comparison with coarse ceramics, the small GS also causes confinement resulting in off-Brillouin zone center $k \neq 0$ phonons and a change in the spectral distribution of the Raman modes. As a result, an additional broadening and shifting of modes are expected in the nanocrystalline ceramics[32] together with possible shifts towards lower/higher frequencies caused by tensile/compressive local stresses. Due to these effects, the allocation of vibration modes to each observed band is even more difficult and to some extent, arbitrary. In spite of this, the main lattice dynamics characteristics and evidence of the phase transitions in the present nanocrystalline BT ceramics have been obtained by a detailed analysis of the Raman activity at various temperatures.

Spectra collected at various positions were identical and well reproducible in time, proving that at micrometer level the SPS nanocrystalline ceramics are highly homogeneous materials and that the special features are not solely due to surface inhomogeneity or to possible surface stresses. Figs. 7 and 8 show the FT-Raman and the micro-Raman spectra of the ceramic with GS $\approx$ 50 nm (reduced by the Bose–Einstein temperature factor), respectively. The evolution with temperature of the wave numbers of the main Raman modes, calculated using a coupled damped-oscillator model are presented in Fig. 9, and a comparison of the spectra obtained for nanocrystalline and micrometric ceramics with those for the single-crystal at selected significant temperatures are shown in Fig. 10.

The main spectral features in these spectra are (a) two intense broad bands A1(TO1) in the range 253–265 cm$^{-1}$ (stiffened component of the soft mode) and A1(TO4) at $\sim$513 cm$^{-1}$; (b) a sharp peak (IR-inactive "silent mode") at $\sim$306 cm$^{-1}$ (B1;TO3-LO3) and a well resolved band at $\sim$717 cm$^{-1}$ (LO4); (c) a small peak E(TO4) at $\sim$487 cm$^{-1}$ considered a stretching mode due to changes in the length of some Ti–O bonds[28–30] which is detected only in the R and O phase and vanishes into a broad feature (denoted as "Y") for temperatures above 300 K; (d) the peak at $\sim$166 cm$^{-1}$ (denoted as "1") attributed to the rhombohedral E(TO1)/orthorhombic B1(TO1) symmetry and the band "2" at $\sim$170–186 cm$^{-1}$ formed by some unresolved TO2-LO2 modes; and (e) a small broad mode at $\sim$630 cm$^{-1}$ (denoted as "3"), not yet attributed to a phonon vibration.[27] More than one

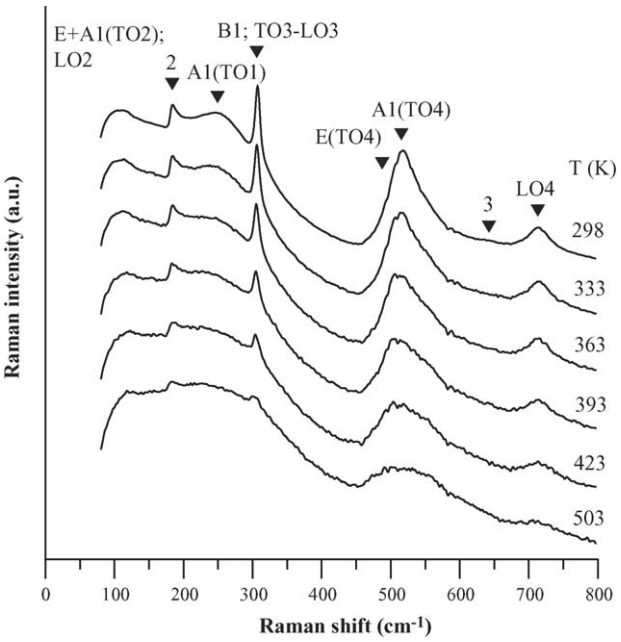


Fig. 7. FT-Raman spectra for the $BaTiO_3$ ceramic sample with average grain size of 50 nm at temperatures in the range 298–503 K.

irreducible phonon mode was assigned to the observed peaks due to the very close values of the A1 and E modes and due to the impossibility of selecting the modes in the unpolarized spectra of the present polycrystalline ceramics. With increasing temperature, a regular broadening and decreasing of intensity is observed together with a softening of the main modes. The modes in the range (200, 350) cm$^{-1}$ and (450, 650) cm$^{-1}$ merge into broad features (denoted as "X", "Y" and "Z"). Unlike the behaviour for single-crystals,[28–31] few modes (B1/TO3-LO3, LO4 and the band "2") persist at temperatures few hundreds

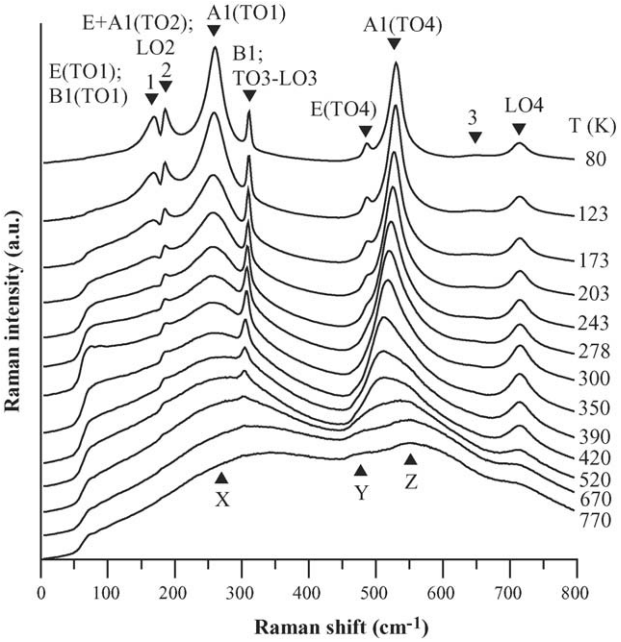


Fig. 8. Micro-Raman unpolarized spectra for the $BaTiO_3$ ceramic sample with average grain size of 50 nm at temperatures in the range 80–770 K.

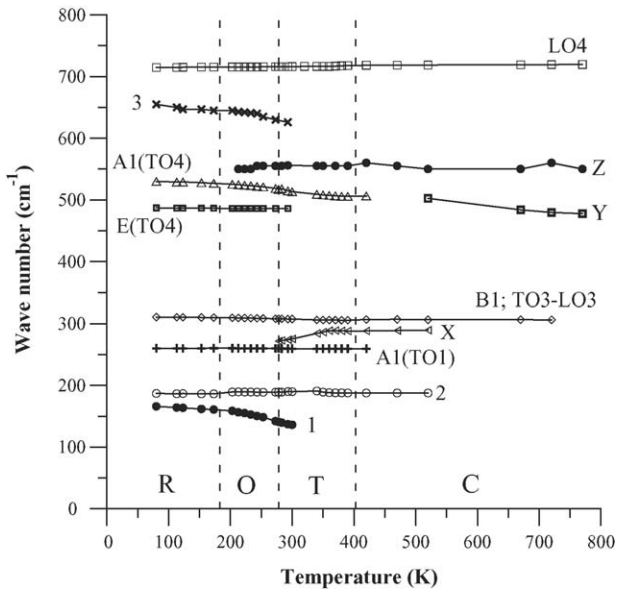


Fig. 9. The evolution with temperature of the wave numbers of the main Raman modes of the $BaTiO_3$ ceramic with average grain size of 50 nm.

degrees above the T–C phase transition (Figs. 8 and 10d). The presence of these bands well above the ferro–para phase transition was also confirmed by the FT-Raman spectra collected from the crushed sample; the behaviour was reproducible after successive heating/cooling cycles (Fig. 7). Thus, it appears that residual stresses, possibly related to polishing or surface contamination coming from the SPS treatment, are not responsible for the persistence of the Raman bands above $T_C$. More likely, it is due to the broken translation symmetry due to the high density of GBs, defects or by short-range polar order (superparaelectric state) regions existing even in the cubic state, as commonly reported for relaxor materials.[36] It seems that the overall properties of the system are strongly affected by a large percentage of regions with frozen polarization, which are assumed to be located at GBs. This interpretation is motivated by the specific dielectric properties of the GB region in $BaTiO_3$, as extensively discussed in recent works.[8,10,38] Evidence of the existence of non-switchable (non-ferroelectric) and field-induced switchable regions besides the normal ferroelectric areas in the present ceramics was provided by a piezoresponse force microscopy study;[11] this gives an idea of the complex local properties in this system. A frozen polar character of the GB regions, as reported for other systems like $SrTiO_3$,[37] can be responsible for the symmetry breaking of

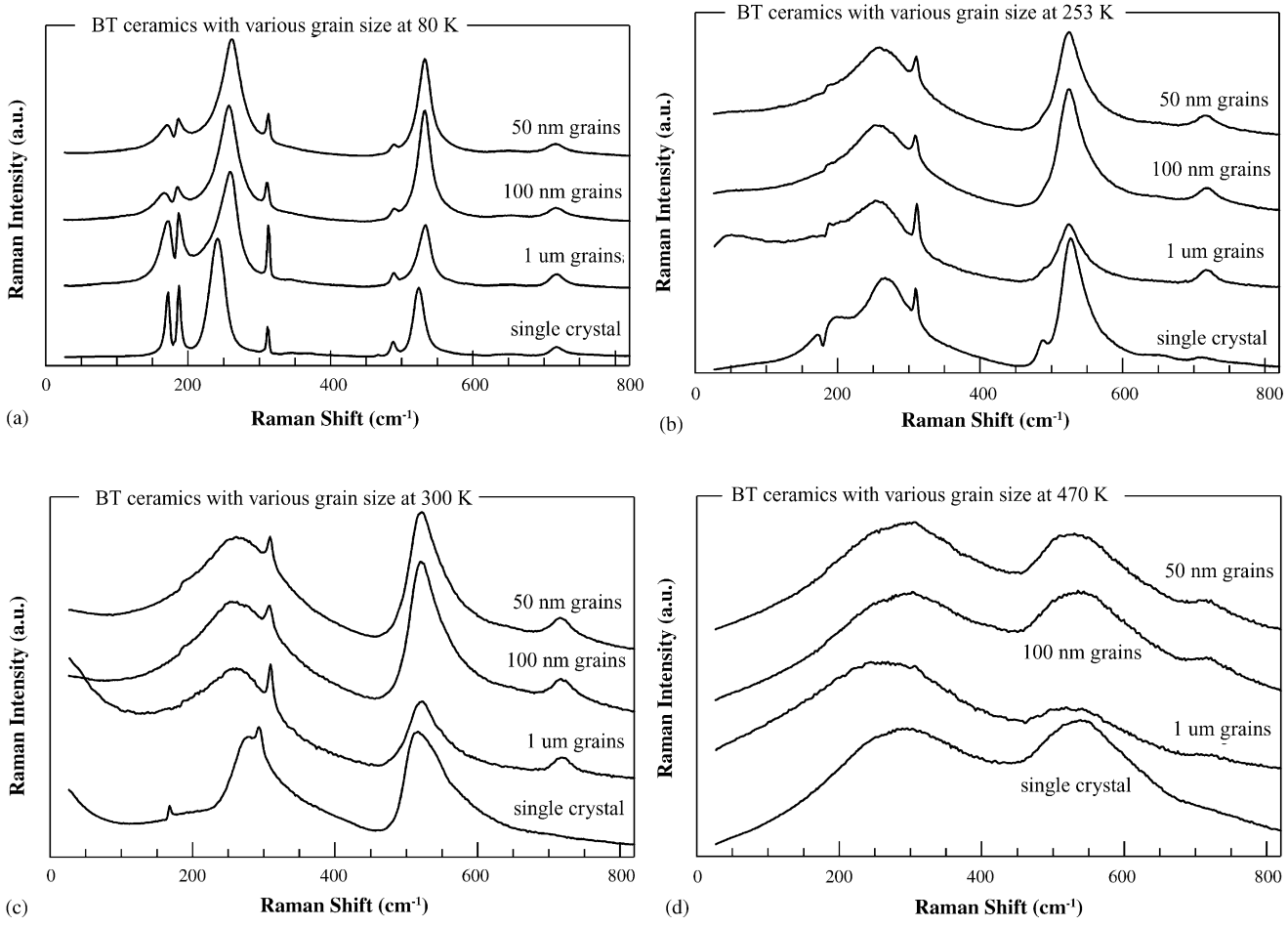


Fig. 10. Comparison between the micro-Raman spectra of $BaTiO_3$ ceramics with various grain sizes and single-crystal at selected temperatures: (a) $T = 80$ K; (b) $T = 253$ K; (c) $T = 300$ K; and (d) $T = 470$ K.

the selection rules in the cubic phase, causing first-order Raman activity at very high temperatures far away from the T–C phase transitions.

The asymmetry of the intense broad modes A1(TO1) and A1(TO4) becomes more evident at high temperatures and was considered in the fits by including the broad features "X", "Y" and "Z", which are increasingly separated as the temperature increases. These broad features are also present in the spectra of single-crystal and coarse ceramics (Fig. 10d). It was previously found that the intensity of the A1(TO1) mode (at $\sim$265 $cm^{-1}$) strongly diminishes around the temperature of 370 K, which was considered as an indication of the Curie temperature,[27] in good agreement with the XRD, DSC and dielectric data.[10] However, more recent results obtained for another group of BT nanocrystalline ceramics did not reveal the same clear evidence, so that this analysis need to be further developed.

The whole micro-Raman spectra obtained for the GS $\approx$ 50 nm ceramics (Fig. 8), which is very similar with one of the sample with GS $\approx$ 100 nm, does not show any dramatic modifications associated with the structural phase transitions of BT, but rather a continuous change of the spectrum from the situation typical of the lower symmetry R phase to that corresponding to highest symmetry C state. Therefore, some instabilities of the spectra in particular ranges of temperatures, the disappearance of modes and anomalies in positions, intensity changes or damping allowed us to conclude that the finest ceramic of this study (GS $\approx$ 50 nm) still exhibits all the structural phase transitions of $BaTiO_3$.[27] Overall, the collected results (XRD, dielectric, calorimetric, Raman) confirm the tendency of phase transitions to become more diffuse at small GS. As Fig. 10(a–d) show, there are no evident differences between the Raman spectra of the nanocrystalline (with 50 and 100 nm GS) and those of coarse (GS $\approx$ 1000 nm) $BaTiO_3$ ceramics. Therefore, specific behaviour can be identified, particularly by comparing with the spectra of single-crystals:

(a) At low temperature (Fig. 10a), the relative intensity of the A1(TO1) peak and the modes denoted as "1" and "2" in Fig. 8 strongly increase with reducing GS (this ratio is <2 for the single-crystal, $\sim$2 in the coarse ceramic and >3 in the fine nanocrystalline ceramics). Particularly, mode "1" is very sharp and intense for the single-crystal, but slightly reduced in intensity and broadened for the coarse ceramics and strongly reduced in the spectra of nanoceramics. Since this mode is for the vibration of Ti against the distorted oxygen octahedron, and its intensity is connected with the distortion of the unit cell (and polarization),[39] the lowering of its intensity with decreasing GS is a consequence of the reduction of the acentric distortion in the fine-grained structures.

(b) The intensity of the mode LO4 is inversely related to GS, particularly at temperatures of 253, 300 and 470 K (Fig. 10c and d). The modes LO4 and B1;TO3-LO3 completely vanish at 470 K in the spectra of the single-crystal while they are still present in case of ceramics. They are probably activated by polar regions, and still present even at high temperatures at the GB regions.

(c) At $T$ = 300 K, a softening of the component A1(TO1) is observed for ceramics in comparison with the single-crystal (Fig. 10c). According to mean-field and self-consistent model calculations,[40,41] the frequency of this soft mode component in the T phase of the perovskite ferroelectrics is proportional to the spontaneous polarization. Since for the present nanocrystalline ceramics, a gradual reduction of the tetragonal distortion with decreasing GS occurred, we expected to find a corresponding reduction of the frequency of the A1(TO1). Practically, there is only a softening in the ceramics in comparison with the single-crystal, but the differences between the coarse and very fine-grained ceramics are not very evident.

(d) There was no evidence of GS effects on the spectral regions of modes "1" and "2" at room temperature (Fig. 10c), considered by other authors,[15,17] to support the idea of a predominant O phase instead of the T one in ultrafine ceramics. There was a strong reduction of mode "2" in passing from the single-crystal to the ceramic state. There were evident differences at $T$ = 253 K where the single-crystal is O (Fig. 10b), and a strong reduction of peaks "1", "2", and the antiresonance dip between them, when reducing the GS. This antiresonance dip was considered as a signature of the T phase,[15] while a positive peak at $\sim$193–196 $cm^{-1}$ was strictly attributed to the O phase.[15,17] In the present ceramics, there were no significant changes in the room temperature data as GS is reduced. More probably, some of the small differences in this range of frequencies can arise from contributions from the GBs. Due to the ambiguity in interpretation of the complex spectral region 170–186 $cm^{-1}$ (including the interpretation of the band "2" and of the antiresonance feature), it is practically impossible to establish the crystalline symmetry on the basis of the comparison of selected bandshapes at fixed temperatures alone. Rather, the evolution with temperatures of all the modes and particularly the disappearance of E(TO4) confirms that the O–T structural phase transition still takes place (at around 293 K for 50 nm GS), so that at room temperature a predominant T phase (even with some possible O traces) is more probable in the nanocrystalline $BaTiO_3$ ceramics than a predominant or exclusively O one. Thus, the structural phase transitions in nanocrystalline $BaTiO_3$ can be better described as a gradual change of the average symmetry through local coexistence of neighbouring phases over a finite temperature range. From the unpolarized Raman spectra, taking into account the broadening effects and interferences caused by the small GS and, without adequate modeling tools, it is not possible to estimate the relative percentage of the coexisting phases at a given temperature.

## 4. Conclusions

Nanocrystalline $BaTiO_3$ dense ceramics down to a GS of 50 nm were prepared from fine nanopowders by SPS. They show all the structural modifications of single-crystal and coarse ceramics (R, O, T and C), with differences resulting from the high density of grain boundaries. With decreasing GS, the phase

transitions progressively assume a more diffuse character, taking place in a broader temperature range. A shift of the average Curie temperature with decreasing GS towards lower values ($T_C \approx 370$ K in the ceramic with GS $\approx 50$ nm) was found by XRD, dielectric and calorimetric investigation. This behaviour suggests the existence of an intrinsic size effect responsible for the decreasing tetragonality *c/a* with reducing GS. In turn, the progressively reduced *c/a* implies a smaller spontaneous polarization and a lower enthalpy for the ferro–para phase transition, which was indeed demonstrated by DSC data. The persistence of the Raman activity at higher temperatures in nanocrystalline ceramics has been interpreted in terms of the stability of some polar structures in the average cubic phase. These can be ascribed to GB regions with a frozen polar character (non-ferroelectric). The collected results obtained in the present study support the existence of combined intrinsic and extrinsic size effects in dense nanocrystalline $BaTiO_3$ ceramics: the progressive reduction of the spontaneous lattice distortion, heat of transition and Curie temperature support the idea of an intrinsic GS effect. Specific features of the dielectric properties, like the lowering of the permittivity, the strong reduction below 0 °C of the CW temperature and of the Raman activity are ascribed to the existence of polar, but non-ferroelectric GB regions (extrinsic effect). However, the exact nature, origin and structure of the polar character of these GBs and their role in the overall macroscopic properties of the nanocrystalline $BaTiO_3$ ceramics has to be further investigated.

## Acknowledgements

This work was performed in the frame of the European COST 525 Action: Advanced Electroceramics–Grain Boundary Engineering. The Italian Ministry of Education, University and Research (PRIN project), the CNCSIS-MEC Romanian grants and the Grant Agency of the Czech Republic also supported this investigation.

## References

1. Akdogan, E. K., Leonard, M. R. and Safari, A., Size effects in ferroelectric ceramics. In *Handbook of Low And High Dielectric Constant Materials for Applications*, *Vol 2*, ed. H. S. Nalwa. Academic Press, 1999.
2. Ahn, C. H., Rabe, K. M. and Triscone, J. M., Ferroelectricity at the nanoscale: local polarization in oxide thin films and heterostructures. *Science*, 2004, **203**, 488–491.
3. Shaw, T. M., Trolier-McKinstry, S. and McIntyre, P. C., The properties of ferroelectric films at small dimensions. *Ann. Rev. Mater. Sci.*, 2000, **30**, 263–298.
4. Arlt, G., Hennings, D. and de With, G., Dielectric properties of fine-grained barium titanate ceramics. *J. Appl. Phys.*, 1985, **58**, 1619–1625.
5. Zhong, W. L., Wang, Y. G., Zhang, P. L. and Qu, B. D., Phenomenological study of the size effect on phase transitions in ferroelectric particles. *Phys. Rev. B*, 1994, **50**, 698–703.
6. Li, S., Eastman, J. A., Li, Z., Foster, C. M., Newnham, R. E. and Cross, L. E., Size effects in nanostructured ferroelectrics. *Phys. Lett. A*, 1996, **212**, 341–346.
7. Jiang, B. and Bursill, L. A., Phenomenological theory of size effects in ultrafine ferroelectric particles of lead titanate. *Phys. Rev. B*, 1999, **60**, 9978–9982.
8. Frey, M. H., Xu, Z., Han, P. and Payne, D. A., The role of interfaces and an apparent grain size effect on the dielectric properties of ferroelectric barium titanate. *Ferroelectrics*, 1998, **206–207**, 337–353.
9. Polotai, A. V., Ragulya, A. V. and Randall, C. A., Preparation and size effect in pure nanocrystalline barium titanate ceramics. *Ferroelectrics*, 2003, **288**, 93–102.
10. Zhao, Z., Buscaglia, V., Viviani, M., Buscaglia, M. T., Mitoseriu, L., Testino, A. *et al.*, Grain-size effects on the ferroelectric behavior of dense nanocrystalline $BaTiO_3$ ceramics. *Phys. Rev. B*, 2004, **70**, 024107.
11. Mitoseriu, L., Harnagea, C., Nanni, P., Testino, A., Buscaglia, M. T., Buscaglia, V. *et al.*, Local switching properties of dense nanocrystalline $BaTiO_3$ ceramics. *Appl. Phys. Lett.*, 2004, **84**, 2418–2420.
12. Jona, F. and Shirane, G., *Ferroelectric Crystals*. Dover Publications Inc., New York, 1993.
13. Lines, M. E. and Glass, A. M., *Principles and Applications of Ferroelectric Materials*. Clarendon Press, Oxford, 1977.
14. Fatuzzo, E. and Merz, J., Ferroelectricity. In *Selected Topics in Solid State Physics*, ed. E. P. Wohlfarth. North-Holland Publishing Company, Amsterdam, 1967.
15. Frey, M. H. and Payne, D. A., Grain-size effect on structure and phase transformations for barium titanate. *Phys. Rev. B*, 1996, **54**, 3158–3168.
16. Takeuchi, T., Tabuchi, M. and Kageyama, H., Preparation of dense $BaTiO_3$ ceramics with submicrometer grains by spark plasma sintering. *J. Am. Ceram. Soc.*, 1999, **82**, 939–943.
17. Takeuchi, T., Capiglia, C., Tabuchi, M., Balakrishnan, N., Takeda, Y. and Kageyama, H., Preparation of fine-grained $BaTiO_3$ ceramics by spark plasma sintering. *J. Mater. Res.*, 2002, **17**, 575–581.
18. Husson, E., Raman spectroscopy applied to the study of phase transitions. *Key Eng. Mater.*, 1998, **155–156**, 1–40.
19. Wada, S., Suzuki, T., Osada, M., Kakihana, M. and Noma, T., Change of macroscopic and microscopic symmetry of barium titanate single-crystal around Curie temperature. *Jpn. J. Appl. Phys.*, 1998, **37**, 5385–5393.
20. Mitoseriu, L., Carnasciali, M. M., Piaggio, P. and Nanni, P., Raman investigation of the composition and temperature-induced phase transition in $(1-x)PbFe_{2/3}W_{1/3}O_3 - _xPbTiO_3$ ceramics. *J. Appl. Phys.*, 2004, **96**, 4377–4385.
21. Busca, G., Buscaglia, V., Leoni, M. and Nanni, P., Solid-state and surface spectroscopic characterization of $BaTiO_3$ fine powders. *Chem. Mater.*, 1994, **6**, 955–961.
22. Uwe, H., Lyons, K. B., Carter, H. L. and Fleury, P. A., Ferroelectric microregions and Raman scattering in $KTaO_3$. *Phys. Rev. B*, 1986, **33**, 6436–6440.
23. Lima, K. C. V., Souza Filho, A. G., Ayala, A. P., Mendes Filho, J., Freire, P. T. C., Melo, F. E. A. *et al.*, Raman study of morphotropic phase boundary in $PbZr_{1-x}Ti_xO_3$ at low temperatures. *Phys. Rev. B*, 2001, **63**, 184105.
24. Testino, A., Buscaglia, M. T., Viviani, M., Buscaglia, V. and Nanni, P., Synthesis of $BaTiO_3$ particles with tailored size by precipitation from aqueous solutions. *J. Am. Ceram. Soc.*, 2004, **87**, 79–83.
25. Testino, A., Buscaglia, M. T., Buscaglia, V., Viviani, M., Bottino, C. and Nanni, P., Kinetics and mechanism of aqueous chemical synthesis of $BaTiO_3$ particles. *Chem. Mater.*, 2004, **16**, 1536–1543.
26. Nygren, M. and Shen, Z., On the preparation of bio-, nano- and structural ceramics and composites by spark plasma sintering. *Solid State Sci.*, 2003, **5**, 125.
27. Buscaglia, V., Buscaglia, M. T., Viviani, M., Ostapchuk, T., Gregora, I., Petzelt, J. *et al.*, Raman and AFM piezoresponse study of dense $BaTiO_3$ nanocrystalline ceramics. *J. Eur. Ceram. Soc.*, 2005, **25**, 3059–3062.
28. Perry, C. H. and Hall, D. B., Temperature dependence of the Raman spectrum of $BaTiO_3$. *Phys. Rev. Lett.*, 1965, **15**, 700–702.
29. DiDomenico, M., Wemple, S. H. and Porto, S. P. S., Raman spectrum of single-domain $BaTiO_3$. *Phys. Rev.*, 1968, **174**, 522–530.
30. Osada, M., Kakihana, M., Wada, S., Noma, T. and Cho, W. S., Broken symmetry in low-temperature $BaTiO_3$ phases: strain effects probed by Raman scattering. *Appl. Phys. Lett.*, 1999, **75**, 3393–3395.
31. Baskaran, N., Ghule, A., Bhongale, C., Murugan, R. and Chang, H., Phase transformation studies of ceramic $BaTiO_3$ using thermo-Raman and dielectric constant measurements. *J. Appl. Phys.*, 2002, **91**, 10038–10043.

32. Luspin, Y., Servoin, J. L. and Gervais, F., Soft mode spectroscopy in barium titanate. *J. Phys. C: Solid State Phys.*, 1980, **13**, 3761–3774.
33. Laabidi, K., Fontana, M. D. and Jannot, B., Underdamped soft phonon in orthorhombic $BaTiO_3$. *Solid State Commun.*, 1990, **76**, 765–768.
34. Last, J. T., Infrared-absorption studies on barium titanate and related materials. *Phys. Rev.*, 1957, **105**, 1740–1750.
35. Dobal, P. S., Dixit, A., Katiyar, R. S., You, Z., Guo, R. and Bhalla, A. S., Micro-Raman scattering and dielectric investigations of phase transition behavior in the $BaTiO_3$–$BaZrO_3$ system. *J. Appl. Phys.*, 2001, **89**, 8085–8091.
36. Ye, Z. G., Relaxor Ferroelectric complex perovskites: structure, properties and phase transitions. *Key Eng. Mater.*, 1998, **155–156**, 81–122.
37. Petzelt, J. *et al.*, Dielectric, infrared, and Raman response of undoped $SrTiO_3$ ceramics: evidence of polar grain boundaries. *Phys. Rev. B*, 2001, **64**, 184111.
38. Emelyanov, A. Yu., Pertsev, N. A., Hoffman-Eifert, S., Böttger, U. and Waser, R., Grain-boundary effect on the Curie–Weiss law of ferroelectric ceramics and polycrystalline thin films: calculation by the method of effective medium. *J. Electroceram.*, 2002, **9**, 5–16.
39. Freire, J. D. and Katiyar, R. S., Lattice dynamics of crystals with tetragonal $BaTiO_3$ structure. *Phys. Rev. B*, 1998, **37**, 2074–2085.
40. Gillis, N. S. and Koehler, T. R., Phase transitions in a model ferroelectric. *Phys. Rev. B*, 1972, **5**, 1925–1932.
41. Pytte, E., Theory of perovskite ferroelectrics. *Phys. Rev. B*, 1972, **5**, 3758–3769.